Eigenchannel R-matrix calculation of the photoabsorption spectrum of strontium

J. Phys. B: At. Mol. Phys. **20** (1987) 6507-6529. Printed in the UK

Eigenchannel *R*-matrix calculation of the photoabsorption spectrum of strontium

Mireille Aymar

Laboratorie Aimé Cotton, CNRS II, Bâtiment 505, 91405 Orsay Cedex, France

Received 23 June 1987

Abstract. This paper presents the first detailed theoretical calculation of the absorption spectrum of Sr out of the $5s^2\,{}^1S_0$ ground state. The autoionisation region below the $5p_{3/2}$ threshold is investigated, photoionisation cross sections being calculated by combining the multichannel quantum defect theory (MQDT) with the eigenchannel *R*-matrix method. Small-scale variational *R*-matrix calculations enable one to evaluate *LS*-coupled short-range reaction matrices. A *jj*-coupled reaction matrix is then deduced using a geometrical frame transformation. Diagonalisation of this matrix gives the energy-dependent MQDT parameters required for the description of the 13 relevant interacting channels. The 13-channel MQDT model built with theoretical *R*-matrix parameters provides an accurate description of the positions and the shapes of the $4d_{3/2,5/2}np$, nf and $5p_{1/2,3/2}ns$, nd $J=1$ autoionising lines. Particular attention is paid to high lying resonances observed near the spin-orbit split $4d_{3/2,5/2}$ and $5p_{1/2,3/2}$ thresholds. Besides obtaining a successful description of the observed absorption spectrum, effects of strong channel mixing are analysed thus providing a deeper understanding of electron correlations in Sr.

1. Introduction

In a previous paper (Aymar *et al* 1987, hereafter to be referred to as I), it was shown that perturbed Rydberg series of Sr can be accurately described by combining the eigenchannel *R*-matrix method (Greene 1983, 1985, O'Mahony and Greene 1985) and the multichannel quantum defect theory (MQDT) (Seaton 1983, Fano and Rau 1986). Similar procedures have been previously used to analyse channel coupling in Be and Mg spectra (O'Mahony and Greene 1985, O'Mahony 1985, O'Mahony and Watanabe 1985) and more recently to describe the photoabsorption spectrum ${}^1P_1^o$ of Ca (Greene and Kim 1987).

This paper is devoted to the photoabsorption spectrum $5s^2\,{}^1S_0$-$J=1^\circ$ below the $5p_{3/2}$ threshold. To our knowledge, there does not exist any theoretical calculation of this spectrum while several theoretical investigations have been devoted to the analogous spectra of Ca (Altun *et al* 1983, Scott *et al* 1983, Greene and Kim 1987) and Ba (Bartschat *et al* 1986). It is thus of particular interest to obtain a quantitative theoretical interpretation of the numerous observations performed by Garton and Codling (1968), Garton *et al* (1968), Hudson *et al* (1969), Connerade *et al* (1980) and Brown *et al* (1983). The absorption spectrum below the $5p_{3/2}$ threshold is dominated by broad $4d_{3/2,5/2}nl$ and $5p_{1/2,3/2}n'l'$ resonances corresponding to the simultaneous excitation of the two 5s electrons. The observed features reflect strong interactions

0022-3700/87/246507+23$02.50

amongst the individual doubly excited series and their interference with the $5s\varepsilon p\ ^1P_1$ and $^3P_1$ continua. Analysis of the channel interactions is an integral part of this study.

All previous calculations carried out in Be, Mg (O'Mahony and Greene 1985, O'Mahony 1985, O'Mahony and Watanabe 1985), Ca (Greene and Kim 1987) or Sr (I) with the eigenchannel R-matrix method neglect the spin-orbit interaction and treat the atom in LS coupling. In Sr (I), such a treatment has allowed the anomalous trend of the intensities of the lowest $4dnp\ ^1P_1^o$ ($n \leqslant 7$) resonances to be successfully explained but has been unable to reproduce the complete structure of the $J = 1^\circ$ photoabsorption spectrum.

It is shown in this paper that most of the features observed in the absorption spectrum of Sr are accurately described by extending the previous techniques (I) to include part of the spin-orbit coupling effects. The calculation scheme results from the division of space into two distinct regions where different forces dominate. We separate the volume in space where all electrons interact strongly from that region where one electron escapes to large distances in a Coulomb field. In the reaction zone where both electrons are at about equal distances from the core, the two-electron Schrödinger equation is solved using the R-matrix method; in this reaction volume, electrostatic interactions prevail over the spin-orbit coupling and the atom is treated in LS coupling. Escape of a single electron beyond the reaction volume is accurately described using the MQDT. In the asymptotic region when one electron is far from the core, the electron can distinguish the fine-structure levels of the ionic core and the atom is treated in jj coupling. The use of a geometrical frame transformation (jj-LS) allows one to connect the two sets of channels adapted to the reaction and asymptotic zones.

Section 2 describes the computational procedure. In § 3 we present the calculated MQDT parameters and analyse the channel coupling. Results on the photoabsorption spectrum are detailed in § 4. Finally, concluding remarks are given in § 5. Atomic units are used throughout.

2. Computational procedure

Section 2.1 summarises the gist of the frame transformation theory which circumvents the explicit inclusion of the spin-orbit coupling effects in the Hamiltonian. The rest of the section describes the specific R-matrix procedure and how to combine it with the MQDT method. Readers familiar with these concepts may proceed to § 3.

2.1. The frame transformation

An essential aspect of the eigenchannel MQDT formulation developed by Fano and co-workers (Lu 1971, Lee and Lu 1973, Fano 1975, Fano and Rau 1986) is the recognition of two distinct sets of channels appropriate to the limiting cases of short- and long-range interactions between the electron and the core. When the electron is far from the core the system breaks into alternative dissociation channels i. In these channels the electron is attracted by the weak long-range Coulomb field and the fine structure of the ion stands out; the coupling between the electron and the ion is better described by the jj scheme than by the LS scheme as previously done in I. The second set of channels is obtained by diagonalising the jj-coupled short-range reaction matrix $K^{(jj)}$ or the jj-coupled short-range scattering matrix $S^{(jj)}$. (These matrices are identical

to the matrices $\mathscr{R}$ and χ respectively in Seaton (1983).) One has

$$K_{ij}^{(jj)} = \sum_{\alpha} U_{i\alpha} \tan \pi\mu_{\alpha} U_{\alpha j}^{\dagger} \tag{1}$$

$$S_{ij}^{(jj)} = \sum_{\alpha} U_{i\alpha} \exp(2i\pi\mu_{\alpha}) U_{\alpha j}^{\dagger}. \tag{2}$$

The orthogonal matrix $U_{i\alpha}$ (hereafter called the frame transformation) which connects the dissociation channels i to the $K^{(jj)}$-matrix eigenchannels α describes the change of coupling between the core and the electron when their separation increases. The i channels are strictly jj coupled while no exact coupling characterises the α channels; however the mixing of α channels is mainly due to electrostatic interactions which, in the reaction region, prevail over spin-orbit coupling. Introducing an intermediate basis $\bar{\alpha}$ of strictly LS-coupled channels, the $U_{i\alpha}$ matrix can be factorised in the form

$$U_{i\alpha} = \sum_{\bar{\alpha}} R_{i\bar{\alpha}} V_{\bar{\alpha}\alpha} \tag{3}$$

where the $R_{i\bar{\alpha}}$ corresponding to the standard (jj-LS) transformation accounts for most of the angular recoupling effects.

The results presented in this paper are based on the surmise that spin-orbit interactions can be neglected in the reaction zone. Spin-orbit effects related to the outer excited electron are completely neglected and $V_{\alpha\bar{\alpha}}$ measures the departure of α channels from LS-coupled $\bar{\alpha}$ channels due to electrostatic interaction only. The validity of this assumption has been discussed by Seaton (1983) from a general point of view and by Aymar (1984) for the alkaline earths. In fact, the major support for the validity of this surmise comes from the quality of the results when compared with experimental data.

The concept of frame transformation between the eigenchannels at small distance r and the dissociation channels at large r has been fruitfully exploited in many different contexts involving atoms, molecules or negative ions in field-free situations or in the presence of external fields (Fano and Rau 1986, Greene and Jungen 1985, Watanabe 1986). In this work the use of the frame transformation added to the assumption of negligible spin-orbit effects in the reaction volume allows one to carry out R-matrix calculations of the eigenquantum defects μ_{α} and $V_{\alpha\bar{\alpha}}$ in LS-coupling. These MQDT parameters are determined by diagonalisation of LS-coupled short-range reaction matrices $K^{(LS)}$.

2.2. Eigenchannel R-matrix calculation

In order to implement the frame transformation, three independent R-matrix calculations are required for $^1P^o$, $^3P^o$ and $^3D^o$ symmetries; the previous R-matrix treatment of the $^1P_1$ spectrum (I) has been complemented by additional, if similar, treatments of the $^3P_1$ and $^3D_1$ channels in LS coupling. The $^1P_1$ and $^3P_1$ spectra require a five-channel calculation (5smp, 4dmp, 4dmf, 5pms, 5pmd) while a three-channel calculation (4dmp, 4dmf, 5pmd) is sufficient for the $^3D_1$ spectrum.

For details on the eigenchannel R-matrix procedure see I and the papers of Greene (1983, 1985), O'Mahony (1985) and Greene and Kim (1987). Briefly, the Schrödinger equation is solved within a finite reaction volume (a sphere of radius r_0) in the configuration space. Using trial functions which are linear combinations of known

functions y_k:

$$\Psi = \sum_k c_k y_k \tag{4}$$

a variational solution of the Schrödinger equation is determined by the condition that the normal logarithmic derivative b on the surface S enclosing the reaction volume defined by

$$\partial\Psi/\partial n + b\Psi = 0 \tag{5}$$

is stationary. For each preselected energy E there are as many solutions Ψ_β with eigenvalues b_β as there are open and weakly closed channels, i.e. channels having non-negligible amplitudes on the surface S. The variational solutions Ψ_β are nothing but the eigenstates of the R matrix.

For a given LS symmetry and for each desired energy E, knowledge of the eigenvalues b_β and eigenfunctions Ψ_β enables one to evaluate the $K^{(LS)}_{\bar\alpha\bar\alpha'}$ matrix connecting the various LS-coupled $\bar\alpha$ channels. The procedure (I, Greene 1983, O'Mahony and Greene 1985, Greene and Kim 1987) consists of projecting the ionic state onto the solutions Ψ_β on the surface S to evaluate the escaping electron amplitudes $F_{\bar\alpha\beta}$ in each channel $\bar\alpha$. The $K^{(LS)}$ matrix is then obtained by joining the amplitudes $F_{\bar\alpha\beta}$ to energy-normalised regular and irregular Coulomb functions $(f_{\bar\alpha}, g_{\bar\alpha})$ (Greene *et al* 1979); these functions are evaluated at the photoelectron energy $\varepsilon_{\bar\alpha} = E - E_{\bar\alpha}$ where the $E_{\bar\alpha}$ corresponds to the average spin-orbit Sr^+ $\bar\alpha$ threshold. Diagonalisation of the $K^{(LS)}$ matrix yields the energy-dependent MQDT parameters μ_α and $V_{\alpha\bar\alpha}$ as well as the eigenchannels Ψ_α. Since $K^{(LS)}$ is slowly varying with energy, the R-matrix calculation is performed on a coarse grid of E values.

Let us now briefly recall how the trial functions are chosen in this work. We employ the usual two-electron Hamiltonian

$$H\Psi = (-\tfrac{1}{2}\nabla_1^2 - \tfrac{1}{2}\nabla_2^2 + U(r_1) + U(r_2) + 1/r_{12})\Psi = E\Psi \tag{6}$$

where the Sr^{2+}-e interaction is described by a simple model potential U whose expression is given in I. For each case ($^1P_1$, $^3P_1$ or $^3D_1$) the LS-coupled two-electron basis functions y_k are expressed in terms of one-electron orbitals

$$y_{nl_1^{(p)}ml_2}(\boldsymbol{r}_1, \boldsymbol{r}_2) = \mathscr{A}\Phi^{(p)}_{nl_1}(r_1) F^{nl_1}_{ml_2}(r_2)\, Y_{l_1 l_2 LM}(\boldsymbol{r}_1, \boldsymbol{r}_2)[\chi_{s_1}(1)\chi_{s_2}(2)]^{SM_s} \tag{7}$$

where $\mathscr{A}$ denotes antisymmetrisation.

The total trial wavefunction is given by

$$\Psi(\boldsymbol{r}_1, \boldsymbol{r}_2) = \sum_{nl_1 p m l_2} c_{nl_1^{(p)}ml_2} y_{nl_1^{(p)}ml_2}(\boldsymbol{r}_1, \boldsymbol{r}_2) \tag{8}$$

where the indices nl_1l_2 define a specific channel converging to the Sr^+ nl_1 threshold. Each channel is described by several $y_{nl_1^{(p)}ml_2}$ functions characterised by the additional indices p and m.

The Rydberg or continuum functions $F^{nl_1}_{ml_2}$ correspond to orbitals of the neutral Sr, obtained by solving the single-particle radial equation for $Sr^+ + e$ approximating the bielectronic interaction by the monopole potential caused by the inner electron (Cowan 1981). As detailed in I and various papers (Greene 1983, O'Mahony and Greene 1985, Greene and Kim 1987) two kinds of orbital $F^{nl_1}_{ml_2}$ are used which either vanish at $r = r_0$ or have a non-zero amplitude at $r = r_0$.

Let us now consider the functions $\Phi^{(p)}_{nl_1}$ which describe the inner electron. The amplitude of these functions is forced to vanish at $r = r_0$ since we assume that both electrons cannot escape from the reaction volume simultaneously. The 5smp and 5pml channels are well represented using a unique $\Phi^{(1)}_{nl_1}$ function which corresponds to the

Sr^+ nl_1 orbital. On the contrary, we have found it essential to introduce two different types of $\Phi_{nl_1}^{(p)}$ functions to accurately describe the 4dml channels. Indeed, the valence electron of Sr^+ can polarise and relax in response to the outermost electron and these effects are particularly important for the 4d orbital of Sr (Griffin *et al* 1969, Connerade *et al* 1980). The set of basis functions $y_{4d^{(1)}ml}$ is complemented by a set of functions $y_{4d^{(2)}ml}$ involving a relaxed 4d′ orbital corresponding to the neutral Sr and $F_{ml_2}^{4d}$ functions with zero amplitude at $r = r_0$. The 4d′ orbital supplies the necessary flexibility to describe the different terms (core relaxation, polarisation, ...) where the 4d electron is less tightly bound than in Sr^+.

Typically, a good description of 5smp and 5pml channels is thus obtained using nine $y_{nl_1^{(1)}ml_2}$ functions, six among them being confined in the reaction volume whereas the 4dml channels are described by nine $y_{4d^{(1)}ml}$ and five $y_{4d^{(2)}ml}$ functions.

At this point we want to compare our treatment with that recently done by Greene and Kim (1987) in the $^1P_1^o$ spectrum of Ca. These authors express their two-electron basis functions in terms of one-electron ionic orbitals only and account for the distortion of these wavefunctions by including in their variational calculation a great number of 'strongly closed' channels converging to highly excited thresholds. Of course, such channels described by functions entirely confined in the reaction volume do not increase the number of R-matrix eigenstates. A second difference concerns the size of the reaction volume: our value $r_0 = 15$ au is smaller than their value $r_0 = 18$ au. Convergence of the variational calculation and of the dipole matrix elements is certainly favoured by such a large value. However this together with the non-inclusion of relaxed orbitals has led Greene and Kim (1987) to take a larger basis set: for the $^1P_1$ spectrum they used 100 functions while in our calculation we have 55 functions only.

2.3. MQDT analyses

Standard techniques of MQDT are described in various papers (Lu 1971, Lee and Lu 1973, Fano and Rau 1986) and only essential points and basic equations are outlined here.

The physical solutions are linear combinations of the $K^{(jj)}$-matrix eigenchannels $\Psi_\alpha(E)$

$$\Psi(E) = \sum_\alpha \Psi_\alpha(E) A_\alpha(E) \tag{9}$$

with the coefficients $A_\alpha(E)$ to be determined by large-r boundary conditions. $\Psi(E)$ must decay exponentially in every closed channel ($i \in Q$) while each open-channel component ($i \in P$) is required to have a common eigenphase shift $\pi\tau_p$. Following Greene and Jungen (1985) and Greene and Kim (1987), the A_α and τ_p are determined from the eigensystem

$$\Gamma' \boldsymbol{A} = \tan \pi\tau \Lambda' \boldsymbol{A} \tag{10}$$

where

$$\Gamma'_{i\alpha} = \begin{cases} U_{i\alpha} \sin \pi(\nu_i + \mu_\alpha) & i \in Q \\ U_{i\alpha} \sin \pi\mu_\alpha & i \in P \end{cases} \tag{11a}$$

$$\Lambda'_{i\alpha} = \begin{cases} 0 & i \in Q \\ U_{i\alpha} \cos \pi\mu_\alpha & i \in P. \end{cases} \tag{11b}$$

Here ν_i is the effective quantum number pertaining to the ith closed channel calculated with respect to the experimental ionisation limit I_i (Moore 1952, Esherick 1977).

At each energy higher than the first ionisation threshold Sr^+ 5s, the number of solutions τ_ρ of system (10) equals the number N_0 of open channels. Each index ρ labels a collision eigenchannel $\Psi_\rho(E)$ characterised by a set of coefficients $A_\alpha^{(\rho)}$. The asymptotic form of $\Psi_\rho(E)$, normalised per unit energy range, is

$$\Psi_\rho(E) = \sum_{i\in P} \Phi_i(f_i(r)\cos\pi\tau_\rho - g_i(r)\sin\pi\tau_\rho)T_{i\rho}(E) + \sum_{i\in Q}\Phi_i P_i(\nu_i, r)Z_i^{(\rho)}(E) \tag{12}$$

where Φ_i represents the ionic state together with the spin and orbital coupling of the outer electron and $P_i(\nu_i, r)$ is an exponentially decreasing Coulomb function (Seaton 1983, Lu 1971). In (12) the coefficients

$$Z_i^{(\rho)} = (-1)^{l+1}\nu_i^{3/2}\sum_\alpha U_{i\alpha}\cos\pi(\nu_i+\mu_\alpha)A_\alpha^{(\rho)} \qquad i\in Q \tag{13}$$

and

$$T_{i\rho} = \sum_\alpha U_{i\alpha}\cos\pi(-\tau_\rho+\mu_\alpha)A_\alpha^{(\rho)} \qquad i\in P \tag{14}$$

describe the relative admixture of dissociation channels. The $A_\alpha^{(\rho)}$ are normalised by the requirement that T be a unitary matrix.

Equations (10) and (11) apply also when all channels are closed, except that the system (10) then possesses a non-trivial solution only at certain energy levels $E^{(n)}$. The mixing coefficients $Z_i^{(n)}$ have the same form as equation (13) with $A_\alpha^{(\rho)}$ replaced by $A_\alpha^{(n)}$ coefficients such that the wavefunction is normalised to unity (Lee and Lu 1973). The $Z_i^{(n)}$ ($Z_i^{(\rho)}$) admixture coefficients of each *jj*-coupled *i* channel into each level (resonance) permit us to determine the admixture coefficients in *LS* or *Jl* coupling. It is thus possible to see what coupling scheme works best for each Rydberg level.

The graphic representation exploited by Lu and Fano (Lu 1971, Fano and Rau 1986) in the discrete spectrum consists of plots of $-\nu_i \pmod 1$ against ν_j for chosen pairs of effective quantum numbers; the direct extension of the Lu–Fano graphs above the *i*th threshold consists of graphs of τ_ρ against ν_j.

Let us now consider the calculation of the oscillator strengths. The density of oscillator strength in the autoionising spectrum is represented as the sum of the contribution corresponding to photoionisation into the N_0 collision eigenstates ρ

$$\frac{\mathrm{d}f}{\mathrm{d}E} = \sum_{\rho=1,N_0}\frac{\mathrm{d}f^{(\rho)}}{\mathrm{d}E} \tag{15}$$

with

$$\mathrm{d}f^{(\rho)}/\mathrm{d}E = \tfrac{2}{3}\omega\,|D_\rho|^2 \tag{16}$$

where ω is the photon energy and D_ρ is defined by

$$D_\rho = \sum_\alpha D_\alpha A_\alpha^{(\rho)}. \tag{17}$$

In equation (17) the D_α are the reduced dipole matrix elements connecting the ground state to the five eigenchannels Ψ_α associated with the $^1P_1$ channels. We use the D_α parameters as previously calculated in I using the length and velocity forms (usual non-relativistic transition operators are employed).

In order to obtain the probability of ejection into a specific dissociation channel *i*, the collision eigenchannels $\Psi_\rho(E)$ must be superposed to eliminate all outgoing wave components in open channels $j \neq i$. The complex superposition coefficients are

$$A_\rho^{i-} = T_{i\rho}\exp(-\mathrm{i}\pi\tau_\rho). \tag{18}$$

The oscillator strength density of the photoelectron which leaves the kth state of the ion behind is

$$\frac{\mathrm{d}f^k}{\mathrm{d}E}=\tfrac{2}{3}\omega\sum_{i\in P_k}\left|\sum_\rho A_\rho^{i-}D_\rho\right|^2 \tag{19}$$

and the total oscillator strength is

$$\frac{\mathrm{d}f}{\mathrm{d}E}=\sum_k\frac{\mathrm{d}f}{\mathrm{d}E}. \tag{20}$$

Finally the total photoionisation cross section is given by

$$\sigma=\frac{4\pi^2}{2(137)}\frac{\mathrm{d}f}{\mathrm{d}E}. \tag{21}$$

3. Eigenchannel MQDT parameters and channel coupling

Figure 1 shows the eigenquantum defects as functions of the energy for the three spectra $^1P_1$, $^3P_1$ and $^3D_1$. The energy dependence is particularly large below the 4d thresholds. For each spectrum, the channels are strongly mixed; the predominant intermediate channel $\bar{\alpha}$ in each eigenchannel α thus depends strongly on the energy.

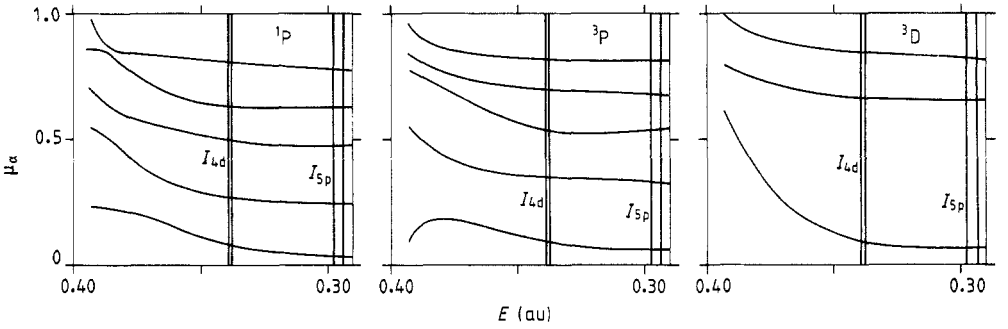

Figure 1. Eigenquantum defects μ_α for the ^1P, ^3P and ^3D spectra as functions of the energy E relative to the double ionisation threshold.

Following Greene and Kim (1987) we analyse the channel interaction using the short-range scattering matrix defined by equation (2). Each element measures the probability that an electron which collides with the target ion Sr^+ in channel i will recoil on channel j. The smooth $S^{(jj)}$ matrix has been constructed from the three R matrices obtained for the $^1P_1$, $^3P_1$ and $^3D_1$ spectra using equation (3) and the known (jj-LS) transformation. The labelling of channels and limits for the complete 13-channel MQDT model are shown in table 1.

The absolute squares of several elements of the $S^{(jj)}$ matrix calculated near either the $4d_j$ or $5p_j$ thresholds are given in table 2. The elements presented there have been selected as representative of the mixing between the nl_1ml_2 and $n'l_1'm'l_2'$ channels corresponding to different configurations. For a given i ($nl_1j_1ml_2j_2$) the channel j ($n'l_1'j_1'm'l_2'j_2'$) corresponds to that which gives the largest $|S_{ij}^{(jj)}|^2$ value. Results are given for particular pairs of (j_1j_2) values but similar results are obtained for other (j_1j_2) pairs.

Table 1. Labels of the channels. The ionisation threshold energies (in cm^{-1}) are referred to the Sr ground state. Shortened symbols used in the figures are indicated between brackets.

	$I_{5s_{1/2}} = 45\,932.19\ cm^{-1}$					
	1	2				
LS	$5snp\ ^3P$	$5snp\ ^1P$				
jj	$5s_{1/2}np_{1/2}$	$5s_{1/2}np_{3/2}$				
Jl	$5s_{1/2}np[\frac{1}{2}]$	$5s_{1/2}np[\frac{3}{2}]$				
	$I_{4d_{3/2}} = 60\,488.09\ cm^{-1}$			$I_{4d_{5/2}} = 60\,768.43\ cm^{-1}$		
	3	4	5	6	7	8
LS	$4dnp\ ^3D$ ($np\ ^3D_1$)	$4dnp\ ^3P$ ($np\ ^3P_1$)	$4dnf\ ^3D$	$4dnp\ ^1P$ ($np\ ^1P_1$)	$4dnf\ ^3P$	$4dnf\ ^1P$
jj	$4d_{3/2}np_{1/2}$	$4d_{3/2}np_{3/2}$	$4d_{3/2}nf_{5/2}$ (nf)	$4d_{5/2}np_{3/2}$	$4d_{5/2}nf_{5/2}$ (nf')	$4d_{5/2}nf_{7/2}$ (nf'')
Jl	$4d_{3/2}np[\frac{3}{2}]$	$4d_{3/2}np[\frac{1}{2}]$	$4d_{3/2}nf[\frac{5}{2}]$ (nf)	$4d_{5/2}np[\frac{3}{2}]$	$4d_{5/2}nf[\frac{1}{2}]$ (nf_1)	$4d_{5/2}nf[\frac{3}{2}]$ (nf_2)
	$I_{5p_{1/2}} = 69\,647.38\ cm^{-1}$		$I_{5p_{3/2}} = 70\,448.84\ cm^{-1}$			
	9	10	11	12	13	
LS	$5pns\ ^3P$ (n)	$5pnd\ ^3D$	$5pns\ ^1P$ (n')	$5pnd\ ^3P$	$5pnd\ ^1P$	
jj	$5p_{1/2}ns_{1/2}$	$5p_{1/2}nd_{3/2}$	$5p_{3/2}ns_{1/2}$	$5p_{3/2}nd_{3/2}$	$5p_{3/2}nd_{5/2}$	
Jl	$5p_{1/2}ns[\frac{1}{2}]$	$5p_{1/2}nd[\frac{3}{2}]$	$5p_{3/2}ns[\frac{3}{2}]$	$5p_{3/2}nd[\frac{3}{2}]$	$5p_{3/2}nd[\frac{1}{2}]$	

Table 2. Absolute squares of selected elements of the short-range scattering matrix.

Near 4d threshold			Near 5p threshold		
i	j	$\lvert S_{ij}^{(jj)}\rvert^2$	i	j	$\lvert S_{ij}^{(jj)}\rvert^2$
$4d_{5/2}np_{3/2}$	$-4d_{5/2}nf_{7/2}$	0.16	$5p_{3/2}ns_{1/2}$	$-5s_{1/2}\varepsilon p_{1/2}$	0.11
	$-5s_{1/2}\varepsilon p_{3/2}$	0.15		$-4d_{5/2}\varepsilon p_{3/2}$	0.09
	$-5p_{3/2}ns_{1/2}$	0.10		$-5p_{3/2}nd_{5/2}$	0.05
	$-5p_{3/2}nd_{5/2}$	0.08		$-4d_{5/2}\varepsilon f_{5/2}$	0.01
$4d_{5/2}nf_{7/2}$	$-5p_{3/2}nd_{5/2}$	0.56	$5p_{3/2}nd_{5/2}$	$-4d_{5/2}\varepsilon f_{7/2}$	0.52
	$-4d_{5/2}np_{3/2}$	0.16		$-5s_{1/2}\varepsilon p_{3/2}$	0.09
	$-5s_{1/2}\varepsilon p_{3/2}$	0.08		$-4d_{5/2}\varepsilon p_{3/2}$	0.08
	$-5p_{1/2}ns_{1/2}$	0.02		$-5p_{1/2}ns_{1/2}$	0.06

By far the strongest mixing corresponds to the $4dmf$-$5pmd$ one (~56-52%) between the 4d and 5p thresholds; similar strong mixing (~60%) was found by Greene and Kim (1987) between the $3dmf$ and $4pmd$ channels of Ca. This unusually strong mixing manifests itself in the very large autoionisation widths of the $5pnd$ resonances, as discussed later. The other channel interaction strengths are weaker; moreover the $4dmp$-$5s\varepsilon p$ mixing is about two times smaller than the analogous mixing in Ca.

4. Absorption spectra

A schematic diagram of the doubly excited series 4dnl and 5pnl' $J = 1$ or Sr is given in figure 2 (see also table 1). The eleven channels converging to the $4d_{3/2,5/2}$ and $5p_{1/2,3/2}$ thresholds interact with the two open channels $5s\varepsilon p\ ^1P_1$ and $5s\varepsilon p\ ^3P_1$ and these interactions produce autoionisation.

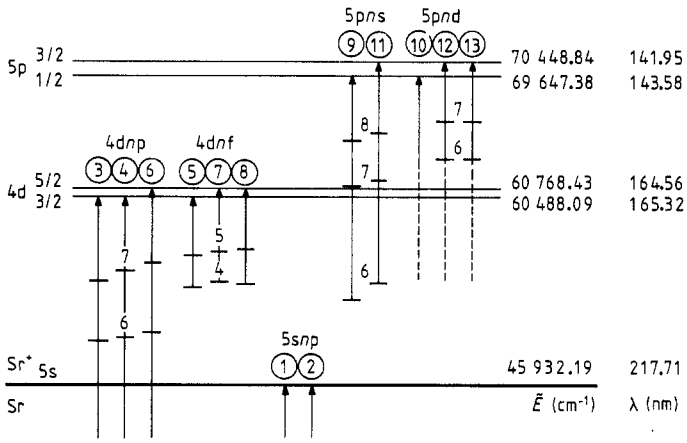

Figure 2. Schematic diagram of the $J = 1$ odd-parity autoionising spectrum of Sr below the $5p_{3/2}$ threshold. Energies $\tilde{E}$ (in cm^{-1}) and wavelengths λ (in nm) are referred to the Sr ground state. See table 1 for the channel labels 1 through to 13.

The absorption spectrum below the $5p_{3/2}$ threshold has been investigated by various experimentalists. The observations of Garton and Codling (1968), Garton *et al* (1968) and Hudson *et al* (1969) concern only the range below the $4d_{5/2}$ limit; the 5pns and 5pnd series were investigated by Connerade *et al* (1980). Finally the absorption spectrum in the 140–190 nm range was reinvestigated by Brown *et al* (1983) with higher spectral resolution. Absolute photoionisation cross sections were obtained by Hudson *et al* (1969) and Lutjens (1973). Comparison of our theoretical results with these various experimental data will be presented successively in different regions of the spectrum. Sections 4.1 and 4.3 concern the large portions of the spectrum between the 5s and $4d_{3/2}$ thresholds and between the $4d_{5/2}$ and $5p_{1/2}$ thresholds respectively; §§ 4.2 and 4.4 deal with the small energy ranges between the two 4d ($4d_{3/2}$ and $4d_{5/2}$) thresholds and the two 5p ($5p_{1/2}$ and $5p_{3/2}$) thresholds respectively.

The theoretical curves displayed in the following sections show the photoionisation cross sections (in Mb, 1 Mb = 10^{-18} cm^2), calculated with the velocity form as a function of either the wavelength λ (in nm) or the energy $\tilde{E}$ (in cm^{-1}) of the transition from the ground state. The velocity form results are expected to be more reliable since, as argued often, the velocity form gives a larger weight to the small r range well described by the R-matrix treatment. Convergence of the variational treatment is checked by comparing length and velocity results.

4.1. Absorption spectrum below the $4d_{3/2}$ threshold

The structure below the $4d_{3/2}$ threshold is due mainly to the 4dnp and 4dnf resonances. In previous works (Garton and Codling 1968, Hudson *et al* 1969) the 4dnp levels have

been identified in the *Jl* and *LS* coupling schemes while *Jl* symbols have been employed for 4d*nf* levels. In addition two observed structures below the $4d_{3/2}$ threshold have been previously assigned to the two lowest members 5p6s $^{1,3}P_1$ of series converging to the $5p_{1/2,3/2}$ thresholds. A final point worth mentioning is the possible existence of the 5p*n*d $^{1,3}P_1$ and $^3D_1$ levels, lowest members of the three 5p*n*d series, within the spectral range below the $4d_{3/2}$ threshold; no structure has been ascribed to these levels but some propositions about their positions can be found in the literature (Garton and Codling 1968, Connerade *et al* 1980, Brown *et al* 1983).

In the region of interest here, the only interpretation of experimental features accounting for channel interactions is due to a qualitative study performed by Brown *et al* (1983). They carried out a graphic analysis of the mixing between the six channels 4d*nl* based on the $4d_{3/2,5/2}$ cores with the help of a hand-sketched Lu–Fano plot drawn through their experimental data. Such an analysis concerns only the positions of the resonances and not their profile; moreover no quantitative information on channel mixing is obtained since the MQDT parameters have not been determined.

We performed two different treatments of this spectral range. The first one, based on an 11-channel MQDT model is somewhat similar to that done by Brown *et al* (1983), i.e. restricted to calculate only the positions of the autoionising lines. The second calculation consists of a complete 13-channel treatment enabling the determination of both the positions and the profiles of the resonances.

4.1.1. Eleven-channel treatment. The MQDT analysis of this subsection is restricted to the closed channels. It involves not only the six 4d*nl* series but also the five 5p*nl'* ones. The corresponding 11-channel MQDT model is built by preventing, though somewhat artificially, the outermost electron from escaping beyond $r = r_0$ in the 5s*m*p channels. For that purpose, we leave out in the variational calculation used to get the *LS*-coupled reaction matrices the trial functions associated with 5s*m*p channels which involve F^{5s}_{mp} orbitals with non-zero amplitude at $r = r_0$. The trial functions which are confined in the reaction volume are however retained in the expansion basis (8). In this way, virtual excitations into the 5s*m*p channels are allowed but the R matrices obtained for the $^1P_1$ and $^3P_1$ spectra have only four eigenstates.

The 11-channel model yields theoretical energies very close to the positions of the absorption peaks calculated with the complete 13-channel model. Likewise, relative admixture coefficients provided by both treatments are very similar. The advantage of the 11-channel model lies in the graphic analysis of the channel mixing and this will be exploited now.

The projection of the theoretical four-dimensional Lu–Fano plot on the $(\nu_{4d_{5/2}}, -\nu_{4d_{3/2}} \pmod 1)$ plane is displayed in figures 3 and 4(*a*). The graph of figure 4(*a*), corresponding to high lying 4d*nl* levels with $43 < \nu_{4d_{3/2}} < 68$ is compared with the tentative Lu–Fano plot drawn by Brown *et al* (1983) through their experimental data with $\nu_{4d_{3/2}} > 15$. Crosses on figure 3 correspond to experimental positions of the resonances while crosses, dots and plus signs on figure 4(*a*) indicate theoretical energies. Some obvious departures appear in figure 3 between theoretical and experimental energies, particularly for $4 < \nu_{4d_{5/2}} < 5$; likewise discrepancies occur between the theoretical curve displayed in figure 4(*a*) and that drawn by Brown *et al* (1983) (figure 4(*b*)). However the overall agreement is quite satisfactory. As already stressed by Brown *et al* (1983), the channel structure pattern considerably changes with increasing energy and this marked evolution is well reproduced by our calculation. This trend is due mainly to the energy dependence of the MQDT parameters (see figure 1) and to

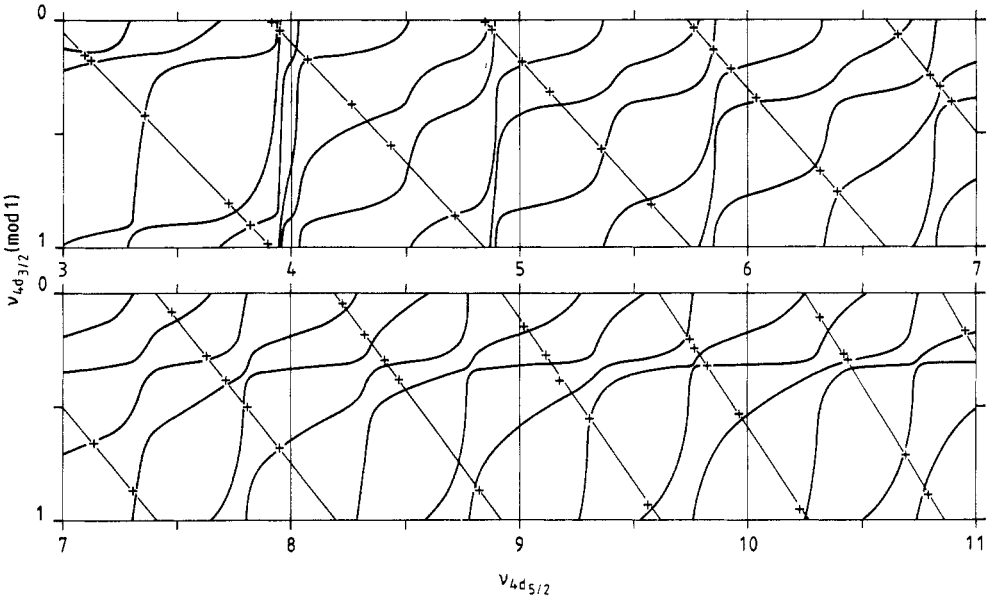

Figure 3. Lu-Fano plot $-\nu_{4d_{3/2}}(\text{mod } 1)$ against $\nu_{4d_{5/2}}$ below the $4d_{3/2}$ threshold: ——, 11-channel calculation; +, experimental resonance positions (Hudson *et al* 1969, Brown *et al* 1983).

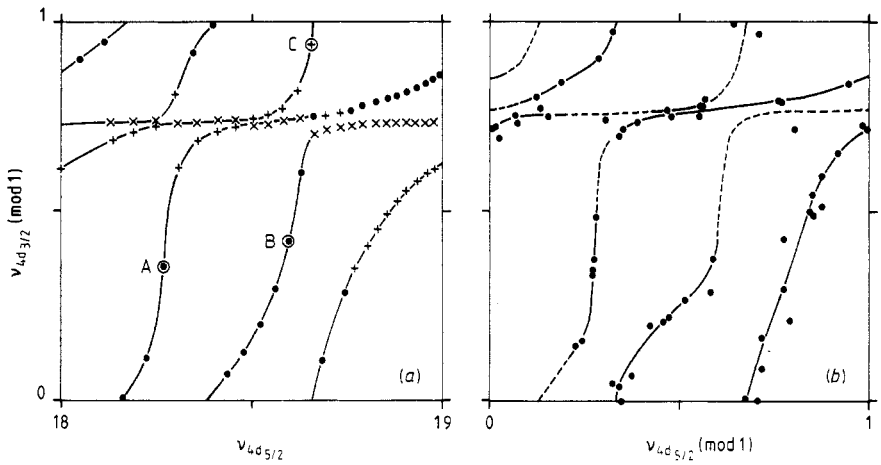

Figure 4. Lu-Fano plot for highly excited 4dnp and 4dnf levels: (*a*) ——, 11-channel calculation, theoretical energy levels with $43 < \nu_{4d_{3/2}} < 68$: ●, $4d_{3/2}nf_{5/2}$; +, $4d_{3/2}np_{1/2}$; ×, $4d_{3/2}np_{3/2}$; A, B and C correspond to the $4d_{5/2}21p_{3/2}$, $4d_{5/2}19f_{5/2}$ and $4d_{5/2}19f_{7/2}$ levels respectively. (*b*) Hand-sketched Lu-Fano diagram drawn by Brown *et al* (1983) through their observed absorption features with $\nu_{4d_{3/2}} > 15$.

the interaction of the 4dnl channels with the 5pnl ones which yields major alterations in the region near $\nu_{4d_{5/2}} \sim 3$-4. The additional vertical segment on the Lu-Fano curve visible near $\nu_{4d_{5/2}} = 4$ corresponds to the presence of the $5p_{3/2}ns$ channel.

The important role played by the 5pnl channels will be analysed in detail in the next section (4.1.2) and here we restrict our discussion to the 4dnl channels. The large avoided crossings between the various nearly horizontal and vertical branches indicate that the 4dnl channels are strongly coupled. Calculation of admixture coefficients $Z_i^{(n)}$ of channels i into each bound level provides quantitative information on the channel mixing, allowing us to determine the best label for each level. In the low-energy range ($\tilde{E} < 58\,100\ \text{cm}^{-1}$, i.e. $\nu_{4d_{5/2}} < 6.5$) our calculation confirms the previous configuration labels of the resonances. However for 4dnp levels LS symbols are more suitable than Jl ones and for 4dnf levels the jj designation is more appropriate than Jl notation. As $\tilde{E}$ increases, the coupling of the 4dnp levels becomes more jj like. However, in the intermediate energy range, assignment of a proper label and even a definite configuration to each level is meaningless due to strong channel mixing. Channel mixing in the high energy range, just below the $4d_{3/2}$ threshold is illustrated in figure 4(a). The $4d_{3/2}np_{1/2,3/2}$ and $4d_{3/2}nf_{5/2}$ high lying Rydberg levels are strongly perturbed by the $4d_{5/2}21p_{1/2}$ and $4d_{5/2}19f_{5/2,7/2}$ levels pertaining to series converging to the $4d_{5/2}$ limit; these latter levels are spread out over many $4d_{3/2}nl$ levels with a maximum admixture of about 10% in the levels denoted A, B and C.

4.1.2. Thirteen-channel treatment. In figure 5, the total photoionisation cross sections computed with the velocity form are compared with the experimental results of Hudson *et al* (1969). The four parts (a)-(d) correspond to decreasing wavelength, i.e. increasing energy; each figure consists of an upper experimental curve and a lower theoretical one. The resonance positions, as measured by Hudson *et al* (1969) or equivalently by Brown *et al* (1983) are depicted by vertical bars; the only additional resonance ($\lambda = 184.59$ nm) detected by Brown *et al* (1983) in the 203-167.7 nm region is indicated in both the upper and the lower frames of figure 5(b) by an arrow. The labels indicated on the upper and lower curves correspond respectively to the previous assignments (Garton and Codling 1968, Hudson *et al* 1969) and to the identifications resulting from our calculations. Shortened symbols, summarised in table 1, are employed. In the low-wavelength range (figure 5(d)) the resonances are so intermixed that labels are meaningless.

We see in figure 5 a good overall agreement between theory and experiment for the positions and widths of the resonances. Departures between theoretical and experimental positions never exceed 0.8 nm and are often much smaller, mainly in the low-wavelength range. The calculation accurately reproduces the relative magnitudes of the intensities of the three resonances pertaining to a given configuration and similar agreement holds for the relative widths (see, for example, the groups of resonances associated with the configurations 4d6p, 4d8p, 4d5f and 4d6f). The noticeable widths of the 4dnp ^{3}P profiles and of all the 4dnf resonances demonstrate the important role played by the spin-orbit interaction.

The most complicated structures emerge in the 190-183 nm range. All the observed features apart from the broad resonance ($\lambda = 184.59$ nm) observed by Brown *et al* (1983)—absorption/window resonances, unsymmetric narrow resonances, broad resonances—have been previously ascribed to levels of the 5p6s, 4d4f and 4d7p configurations (Garton and Codling 1968, Garton *et al* 1968, Hudson *et al* 1969). In this range all the 13 channels are strongly mixed and resonances interfere and overlap;

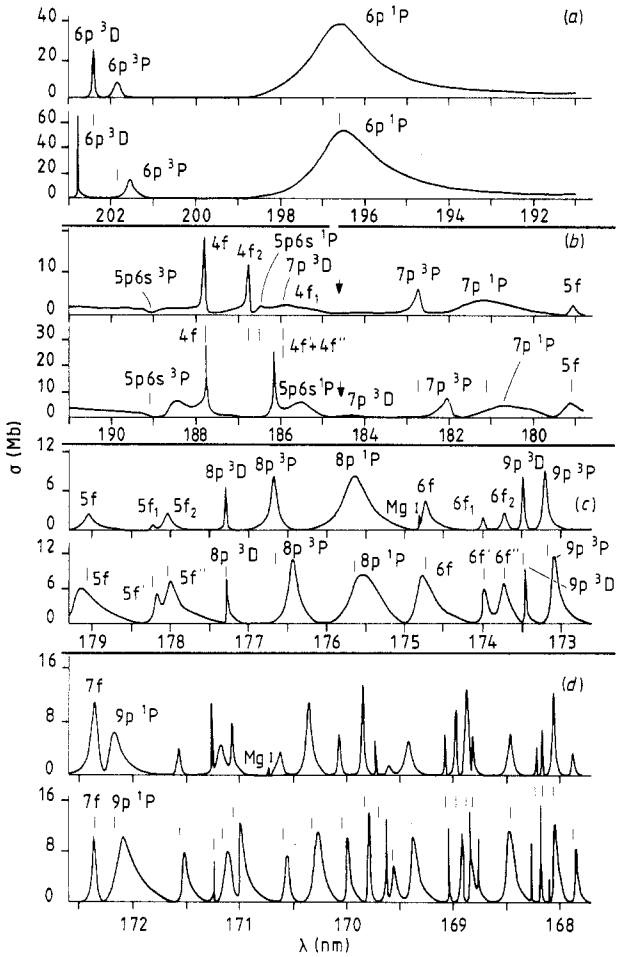

Figure 5. Total photoionisation cross section between the 5s and $4d_{3/2}$ thresholds. For each pair of figures (*a*)-(*d*) the experimental data of Hudson *et al* (1969) (upper curve) are compared with *R*-matrix results (lower curve). Vertical bars and arrows indicate experimental resonance positions as observed by Hudson *et al* (1969) and Brown *et al* (1983). For level assignment see the text and table 1. Cross section scales are different for experimental and theoretical curves.

thus the exact position and shape of the resonance are very sensitive to error. This explains our difficulty in describing the experimental data perfectly. However the main experimental features are correctly reproduced and information on state composition is obtained. Our study confirms that two resonances are ascribable to the 5p6s $^3P_1$ and $^1P_1$ levels. The two narrow and intense peaks correspond to the 4d4f levels, the two $4d_{5/2}4f_{5/2,7/2}$ resonances overlapping to form one single structure. In addition we found a broad and weak resonance at $\lambda = 184.6$ nm (in agreement with the observation of Brown *et al*) which is identified as the 4d7p ^{3}D level.

Our study confirms that the 5p5d levels cannot be ascribed to particular structures. In fact, these levels are completely embedded in several resonances; strong admixture of the 5p*n*d channels is found in numerous resonances, mainly the 4d6p, 4d4f, 5p6s and 4d7p. This particular behaviour of the 5p5d levels results from the strong mixing

of the 5p*n*d channels with other channels, particularly with the 4d*n*f ones (see § 3). As already found in I the large admixture of 5p*n*d character and, to a smaller extent, of 5p*n*s character into the 4d7p $^1P_1$ level explains the anomalous course of intensity along the 4d*n*p $^1P_1$ series. This also explains why the 4d4f resonances are much sharper than high lying 4d*n*f ones, the narrowing of the resonances being certainly due to destructive interferences of the different autoionisation paths. The number of coupled channels is too large to analyse this phenomenon more precisely similar to that observed for the 3d6p $^1P_1$ resonance of Ca (Greene and Kim 1987).

Some comparison with the Ca spectrum should be made here. In Ca also, the 4p4d $^1P_1$ resonance, analogous to the 5p5d $^1P_1$ resonance of Sr, has not been observed (Connerade *et al* 1980). We think that, here again, the oscillator strength of the $4s^2$–4p4d $^1P_1$ transition is distributed throughout several resonances located below the 3d threshold, preventing a particular resonance from being associated with the 4p4d $^1P_1$ level. This interpretation differs from that given by Scott *et al* (1983) who assign the first member of the 4p*n*d series to a resonance above the 3d threshold.

The two last comments concern the comparison between length and velocity results and the absolute magnitudes of the cross sections. Results obtained with the length form are very close to those obtained with the velocity form; some typical values are listed in table 3. The magnitude of the theoretical cross sections at the various peaks is larger than the absolute measurement of Hudson *et al* (1969). However, the reliability of these absolute values has been questioned. From extrapolation of the oscillator strengths of the principal series to the threshold region, Parkinson *et al* (1976) indicate that the photoionisation cross sections of Hudson *et al* (1969) should be increased by a factor of 1.9. Lutjens (1973) estimates that his cross section measurements are a factor of 1.7 higher than those of Hudson *et al* (1969), but caution must be exercised since his experimental uncertainty is about 30%. Our results for 4d*n*p resonances seem to indicate that the experimental values of Hudson *et al* (1969) should be raised but with a somewhat smaller scaling factor than recommended by Parkinson *et al*

Table 3. Comparison of absolute values of the photoionisation cross sections (in Mb) calculated with either the velocity form (*a*) or the length form (*b*) with experimental data (*c*) of Hudson *et al* (1969); *R* indicates the ratio between velocity results and experimental values.

	(*a*)	(*b*)	(*c*)	*R*
4d6p ^1P	54.5	56.0	40	1.4
4d7p ^3P	8.1	8.5	6.4	1.3
4d7p ^1P	4.4	4.2	4.0	1.1
4d8p ^3P	11.2	11.5	7.9	1.4
4d8p ^1P	9.3	9.3	7.9	1.2
4d9p ^3P	12.2	12.8	8.8	1.4
$4d_{3/2}5f_{5/2}$	5.6	6.5	2.4	2.7
$4d_{3/2}6f_{5/2}$	8.4	8.7	4.3	2.0
$4d_{5/2}23p_{3/2}$	4.1	4.7		
$4d_{5/2}21f_{7/2}$	7.3	7.9		
$5p_{1/2}7s_{1/2}$	4.6	5.5		
$5p_{3/2}7s_{1/2}$	2.8	3.2		
$5p_{1/2}8s_{1/2}$	2.9	3.7		
$5p_{3/2}8s_{1/2}$	2.9	3.7		

(1972). Additional absolute measurements in a wider range are worthwhile to clarify the situation.

4.2. Absorption spectrum between the $4d_{3/2}$ and $4d_{5/2}$ thresholds

The absorption lines observed between the $4d_{3/2}$ and $4d_{5/2}$ thresholds by Hudson *et al* (1969) and later by Brown *et al* (1983) with higher spectral resolution have been classified into two spectral series $4d_{5/2}np[\frac{3}{2}]$ ($n \geqslant 23$) and $4d_{5/2}nf[\frac{3}{2}]$ ($n \geqslant 21$) only, although three series are expected in this energy range. Total photoionisation cross sections computed with the velocity form are displayed in figure 6. The positions and widths of resonances are in excellent agreement with experimental results of Brown *et al* (1983) while the relative magnitude of intensity of the peaks is a little less satisfactory. In table 3, it can be seen that the length and velocity results are again very close. Absolute cross section measurements (Hudson *et al* 1969) were done with such a low spectral resolution that reliable comparison with our predictions is not possible.

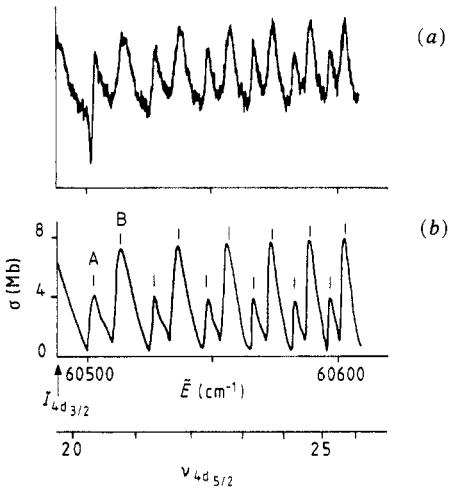

Figure 6. Total photoionisation cross section between the $4d_{3/2}$ and $4d_{5/2}$ thresholds. (*a*) Experimental results of Brown *et al* (1983) in arbitrary units. (*b*) Theoretical results; vertical bars indicate the position of the observed absorption peaks. A and B are the $4d_{5/2}23p_{3/2}$ and $4d_{5/2}21f_{7/2}$ resonances respectively.

Now let us analyse the absence of the third spectral series by studying in detail the oscillator strength density in one unit range of $\nu_{4d_{5/2}}$. The total oscillator strength density is the sum of the contribution of photoionisation to five eigenchannels ρ (equation (15)) characterised by one of the five roots τ_ρ of equation (10). The five eigenphase shifts τ_ρ are plotted in figure 7(*a*) as a function of $\nu_{4d_{5/2}}$. The separate contributions $df^{(\rho)}/dE$ are plotted in figure 7(*b*). Figure 7(*a*) bears visible similarity with figure 4(*a*): in particular, in both figures the three nearly vertical branches near $\nu_{4d_{5/2}}(\text{mod } 1) = 0.15$, 0.35 and 0.65 correspond respectively to the $4d_{5/2}np_{3/2}$, $4d_{5/2}nf_{5/2}$ and $4d_{5/2}nf_{7/2}$ channels. The major difference between figures 4(*a*) and 7(*a*) concerns the presence of two additional nearly horizontal branches in figure 7(*a*); these branches are associated with the two $5s\varepsilon p$ continua disregarded in § 4.1.1. It clearly appears

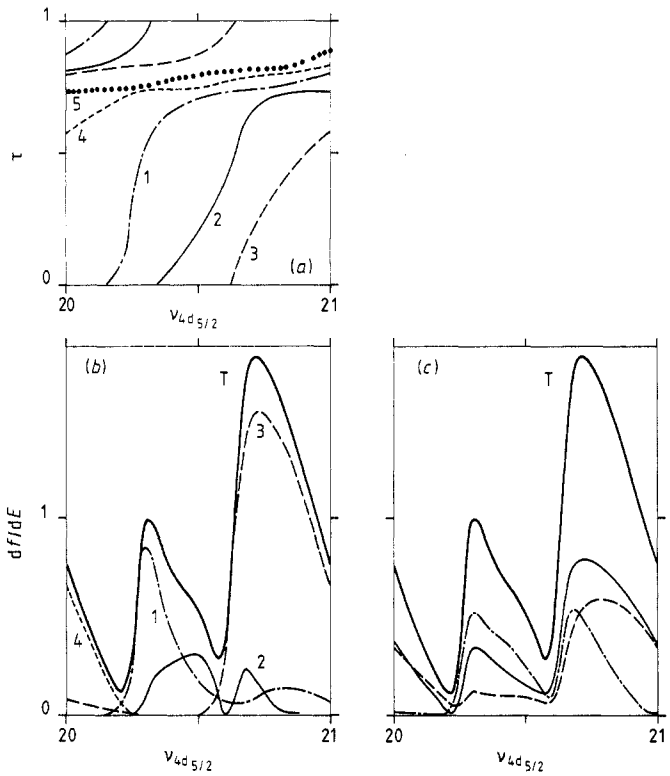

Figure 7. Eigenphase shifts and oscillator strength densities between the $4d_{3/2}$ and $4d_{5/2}$ threshold. (*a*) Eigenphase shifts τ_ρ ($\rho = 1$-5) as functions of $\nu_{4d_{5/2}}$. (*b*) Partial oscillator strength densities $df^{(\rho)}/dE$ for $\rho = 1$-4 ($df^{(5)}/dE \sim 0$) and total oscillator strength density df/dE (T). (*c*) Partial oscillator strength densities for photoionisation to $5s\varepsilon p$ (——), $4d\varepsilon p$ (— — —) and $4d\varepsilon f$ (— · —) continua and total oscillator strength density (T).

that the transitions to the $\rho = 2$ channel have low oscillator strength and that most of the oscillator strength density comes from the eigenchannels $\rho = 1$ and 3, leading to the observation of only two series in the spectral range under study. This interpretation agrees with that previously given by Brown *et al* (1983). However, since the three closed channels $4dnl$ are strongly mixed, the designation $4d_{5/2}np_{3/2}$ and $4d_{5/2}nf_{7/2}$ for the series is only approximate.

In figure 7(*c*) we show partial oscillator strength densities for photoionisation to the $5s\varepsilon p$, $4d_{3/2}\varepsilon p$ and $4d_{3/2}\varepsilon f$ continua. Branching ratios for autoionisation to the various Sr^+ ion cores depend strongly on $\nu_{4d_{5/2}}$, autoionisation through open channels built on the 5s core never being negligible.

4.3. Absorption spectrum between the $4d_{5/2}$ and $5p_{1/2}$ thresholds

The structure of the absorption spectrum between the $4d_{5/2}$ and $5p_{3/2}$ thresholds is due to transitions to the five $5pns$, nd channels. The observations of Connerade *et al* (1980) have been extended and improved by Brown *et al* (1983). No absolute measurement of cross section exists, to our knowledge, in this energy range.

Total cross sections calculated in the 165.3-145 nm range using the velocity form are compared with experimental data in figure 8. Above $\lambda \sim 149$ nm, our calculated

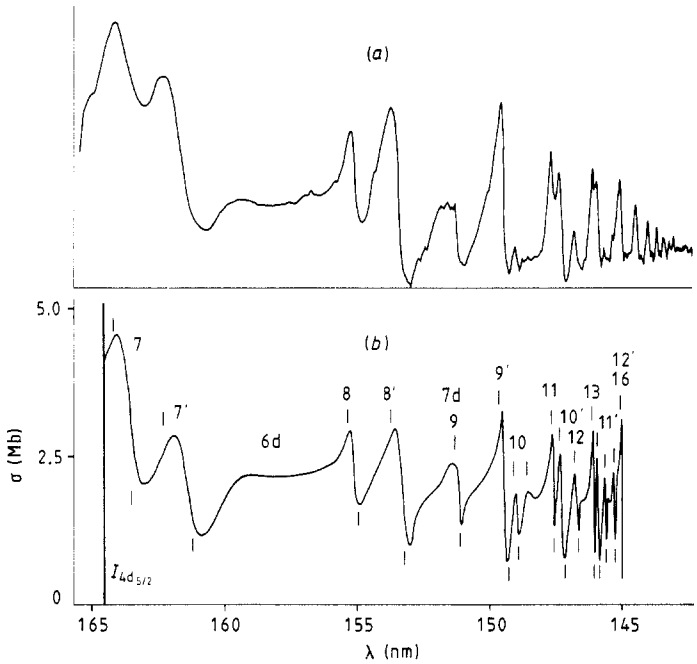

Figure 8. Total photoionisation cross section between the $4d_{5/2}$ and $5p_{1/2}$ thresholds. (*a*) Experimental results of Connerade *et al* (1980) in arbitrary units. (*b*) Theoretical results. Vertical bars above and below the curve indicate the positions of absorption peaks and minima observed by Brown *et al* (1983). For level assignment see the text and table 1.

curve reproduces nicely the experimental spectrum of Connerade *et al* (1980). In the lower wavelength range, the experimental resolution is too low for a precise comparison. Moreover the experimental λ scale being non-linear, the vertical correspondence between the experimental and theoretical curves is only approximate. Thus the positions of the calculated absorption maxima and minima are compared with the corresponding values reported by Brown *et al* (1983). Good agreement is obtained in the whole λ range.

The two imbricated $5p_{1/2}ns$ and $5p_{3/2}ns$ series can be easily identified and labels obtained in this work confirm previous ones (Connerade *et al* 1980). On the other hand, most of the $5pnd$ resonances have too broad an autoionisation width to be recognisable in the structure; this mainly results from the strong coupling of the $5pnd$ channels with the $4d\varepsilon f$ continua. In particular, it is often impossible to distinguish the three members of a given $5pnd$ configuration. Thus, for instance, the three 5p6d (5p7d) resonances merge into one complex and broad feature marked 6d (7d) in figure 8.

Our cross section curve calculated in the 69 100-69 770 cm^{-1} range (144.7-143.3 nm range) is compared with experimental data of Brown *et al* (1983) in figure 9. The overall agreement between theory and experiment is excellent is spite of the complexity of the structure. The various characteristics of experimental resonances (position, width, intensity) are accurately reproduced. As in figure 8, quantum numbers are assigned to $5p_{1/2}ns$ and $5p_{3/2}ns$ levels only; these levels correspond to the sharpest features while the shoulders or broad resonances between the $5pns$ peaks are associated with $5p_{1/2}nd$ or $5p_{3/2}nd$ levels.

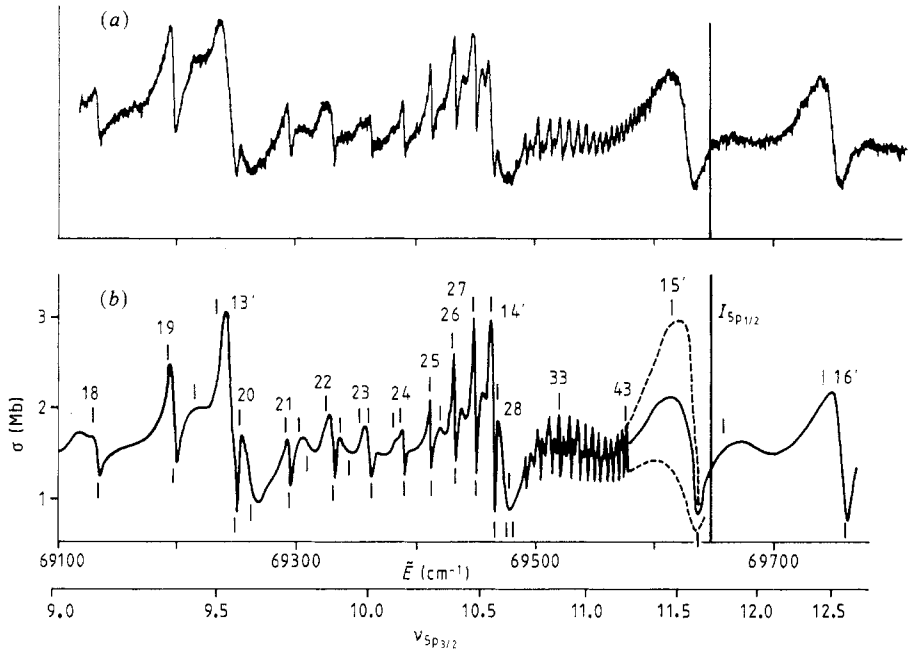

Figure 9. Total photoionisation cross section near the $5p_{1/2}$ threshold: (*a*) experimental results of Brown *et al* (1983) in arbitrary units, (*b*) theoretical results. Vertical bars above and below the curve indicate the positions of absorption peaks and minima observed by Brown *et al* (1983). Just below the $5p_{1/2}$ limit, the broken curves correspond to the envelopes of theoretical maxima and minima and the full curve to the average cross section. For level assignment see the text and table 1.

Agreement between theory and experiment is somewhat better for 5p*nl* series than for 4d*nl'* series (§§ 4.1.2, 4.1.3). However, as visible in table 3, differences between length and velocity results are larger for 5p*n*s resonances. Better convergence was obtained by Greene and Kim (1987) for analogous 4p*nl* series of Ca. Certainly, the two-electron basis set or the size of the reaction volume used in the variational calculation should be increased to improve the convergence.

Recently Ueda (1987) has fitted the portion of the absorption observed by Brown *et al* (1983) in the 69 125–69 535 cm^{-1} energy range to a parametric formula obtained with a simplified three-channel MQDT model which completely disregards the 5p*n*d channels. Comparison of his figure 4 with our figure 9 clearly shows that the observed features are better reproduced by our theoretical calculation.

The intensity of the resonances varies periodically with $\nu_{5p_{3/2}}$, with maximum intensity for the $5p_{3/2}ns$ peaks; the periodic intensity variation is similar to that observed above the $5p_{1/2}$ threshold. Our calculation perfectly reproduces these intensity variations which will be explained in the next subsection.

4.4. Absorption spectrum between the $5p_{1/2}$ and $5p_{3/2}$ thresholds

Connerade *et al* (1980) have classified the lines they observed between the $5p_{1/2}$ and $5p_{3/2}$ thresholds into two series $5p_{3/2}ns[\frac{3}{2}]$ ($n \geq 16$) and $5p_{3/2}nd[\frac{1}{2}, \frac{3}{2}]$ ($n \geq 14$). This spectral range has been reinvestigated by Brown *et al* (1983) with higher spectral

resolution. Figure 10 shows that the asymmetrical absorption/window profiles observed by Brown *et al* (1983) are nicely reproduced by our calculation.

Let us now analyse the shapes of the $5p_{3/2}ns,nd$ resonances in greater detail by studying the evolution of the oscillator strength density in one unit of $\nu_{5p_{3/2}}$. The eigenphase shifts τ_ρ and the separate $df^{(\rho)}/dE$ are plotted in figure 11(a)-(b) as a function of $\nu_{5p_{3/2}}$; only the $df^{(\rho)}/dE$ with $\rho = 1$-5 contributing significantly to the total oscillator strength density are reported in figure 11(b). The shape of the curves displayed in figure 11(a), with large avoided crossings between the various branches and almost no vertical segment, indicates strong channel mixing. The portions of the five curves $\rho = 1$-5 which contribute to the total oscillator strength density cannot be assigned to a particular dissociation channel; this point is illustrated by distinguishing, in the figures 11(a) and (b), for each ρ channel the closed channel i corresponding to the maximum i character. It clearly appears that both resonances are complex mixtures of the three $5p_{3/2}ns,nd$ channels; in other words, the observed autoionising lines represent periodic variation in the composition of the upper-state channel rather than individual transitions to individual upper-state resonance. However, the $5p_{3/2}ns$ character is dominant near $\nu_{5p_{3/2}} = 12.55$ and thus the highest resonances observed between the $5p_{1/2}$ and $5p_{3/2}$ thresholds may be approximately ascribed to the $5p_{3/2}ns$ series and the others to the $5p_{3/2}nd$ series, in agreement with Connerade *et al* (1980).

It is worth noting here that similar asymmetrical absorption/window profiles have been observed also by Brown and Ginter (1978, 1980) near the $4p_{1/2,3/2}$ thresholds of Ca and near the $6p_{1/2,3/2}$ limits of Ba, stressing the great similarity between the heavy alkaline earths.

In figure 11(c) we show the partial oscillator strength densities for photoionisation to the $5s\varepsilon p$, $4d\varepsilon p$, $4d\varepsilon f$ and $5p_{1/2}\varepsilon l$ continua. Autoionisation through the open channels built on the $5p_{1/2}$ core is very small and autoionisation proceeds mainly through the $4d\varepsilon p$ channels. This explains why the periodic intensity variation of the profile above

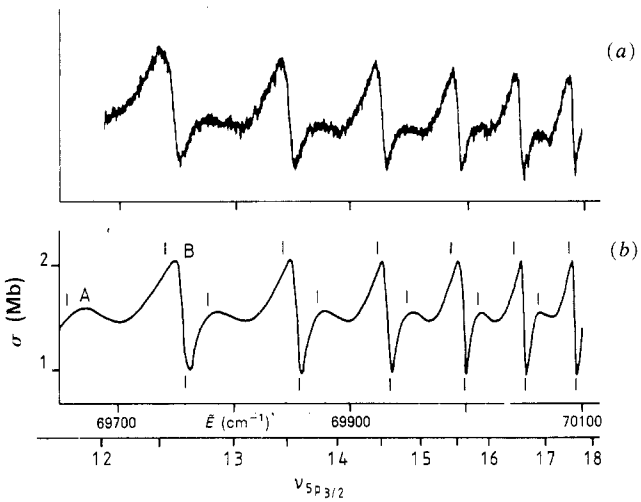

Figure 10. Total photoionisation cross section between the $5p_{1/2}$ and $5p_{3/2}$ threshold: (a) experimental results of Brown *et al* (1983) in arbitrary units, (b) theoretical results. Vertical bars above and below the curve indicate the positions of absorption peaks and minima observed by Brown *et al* (1983). A and B are the $5p_{3/2}14d$ and $5p_{3/2}16s$ resonances respectively.

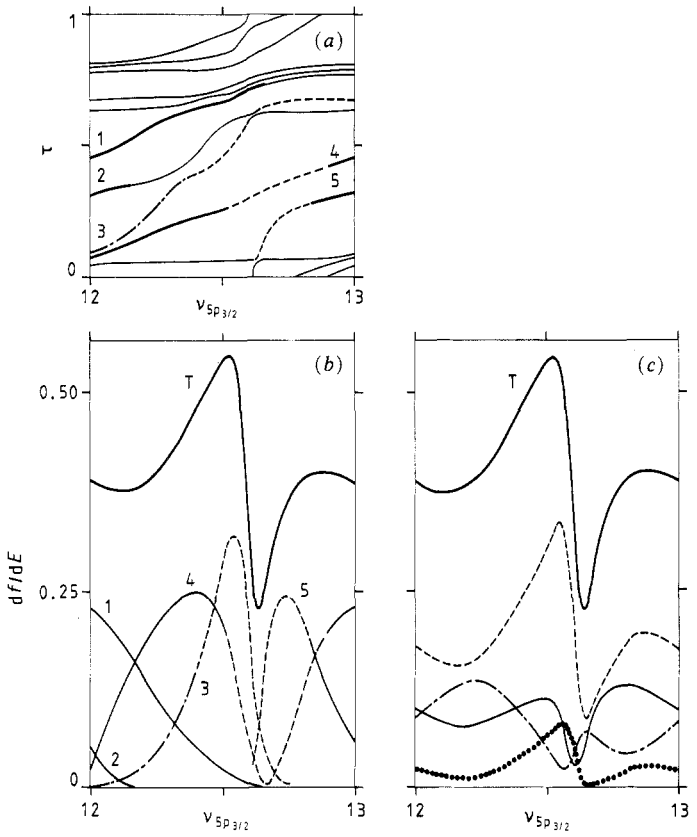

Figure 11. Eigenphase shifts and oscillator strength densities between the $5p_{1/2}$ and $5p_{3/2}$ thresholds: (*a*) eigenphase shifts τ_ρ ($\rho = 1$-10) as functions of $\nu_{5p_{3/2}}$. The closed-channel *jj* characters are: ——, $5p_{3/2}nd_{5/2}$; — - —, $5p_{3/2}nd_{3/2}$; and ---, $5p_{3/2}ns_{1/2}$ (see the text). (*b*) Partial oscillator strength densities $df^{(\rho)}/dE$ for $\rho = 1$-5 ($df^{(\rho)}/dE \sim 0$ for $\rho = 6$-10) and total oscillator strength density df/dE (T). (*c*) Partial oscillator strength densities for photoionisation to $4d\varepsilon p$, ---; $4d\varepsilon f$, — - —; $5s\varepsilon p$, ——; and $5p_{1/2}\varepsilon s,\varepsilon d$, ••••, continua and total oscillator strength density (T).

the $5p_{1/2}$ threshold (figure 10) continues to be evident below the $5p_{1/2}$ threshold (figure 9). Our results on the branching ratio for autoionisation compare well with those obtained in Ca by Scott *et al* (1983) between the Ca^+ 3d and 4p thresholds.

5. Conclusion

The present study demonstrates that a good theoretical description can be obtained for the absorption spectrum of Sr, despite extremely strong correlations between the outer electrons and the severe breakdown of *LS* coupling. Such a success lies in the judicious combination of two complementary methods, namely the eigenchannel *R*-matrix and MQDT theories.

The short-range effects are handled economically by exploiting two concepts introduced by Fano (Fano and Rau 1986), i.e. the physical significance of the smooth short-range reaction matrix and the recognition of the key role played by the frame

transformation $U_{i\alpha}$. R-matrix calculations of the smooth reaction matrix which do not reflect any resonance effects associated with the closed channels are performed on a coarse energy mesh, typically 0.05 au. The assumption of negligible spin–orbit effects in the reaction volume, well justified in view of the quality of the results, reduces the computational time by permitting the R-matrix calculations to be carried out in LS coupling. In addition, the rapid convergence of the variational method developed by Greene (1983, 1985) enables short-range physics to be handled efficiently.

Unlike in most R-matrix calculations, computational effort is not spent in finding eigenfunctions of the Hamiltonian at each desired energy, or equivalently in calculating on a fine energy mesh the physical scattering matrix referring to the open channels only, whose poles determine the resonances. In fact, the eigenchannel R-matrix method links naturally with quantum defect theory, and standard algebraic MQDT procedures have been exploited for calculating physical observables on an arbitrarily fine energy mesh, sometimes smaller than 0.01 cm^{-1}. The 13-channel MQDT model built in this work depends on 41 parameters which strongly depend on energy and it is difficult to envisage how these could have been obtained empirically from experiment. Thus, difficulties often encountered in the empirical MQDT treatment of complex spectra (Aymar 1984) have been bypassed by calculating the short-range parameters.

Moreover, the advantages of the eigenchannel MQDT method have been fully exploited. Graphic representations have been used to sort out channel mixing and the calculation of admixture coefficients of closed channels into each resonance has enabled us to quantitatively analyse channel interactions and to identify the resonances. Thus, in contrast with most photoionisation calculations, our study is not restricted to the determination of the positions, shapes and intensities of the autoionising lines but also provides a deeper understanding of the effects of channel mixing. In particular, the unusually strong 5pmd–4dmf coupling dominates all the $J = 1°$ spectrum of Sr. It is reflected in the uncommon behaviour of the 5p5d levels and in the large autoionisation widths of the 5pnd resonances. Strong channel mixing manifests itself also in a clear breakdown of the independent-particle behaviour. The independent-electron designation fails to label many levels and the remaining question is whether an alternative quantisation could be found to label these levels better. Although some steps toward elucidating this problem have been recently made (Fano 1983, Fano and Rau 1986, Krause and Berry 1985, Berry and Krause 1987), much remains to be done.

All of the alkaline earths share the strong coupling seen for Sr. Some examples, stressing the similarity of Sr with either Ca or Ba have been given in this paper. However a more detailed analysis of systematics in heavy alkaline earths would require additional theoretical investigations. Improved description of the absorption spectrum of Ca near the spin–orbit split thresholds necessitates inclusion of the spin–orbit coupling effects. The procedure used in this paper for handling Sr is expected to work in Ca and the corresponding treatment of Ca has been undertaken by Kim and Greene (1987). For Ba, spin–orbit effects are much more important and they must be considered within the reaction zone. An R-matrix calculation which includes relativistic terms in the Hamiltonian has been carried out by Bartschat *et al* (1986), but this study was restricted to a limited number of resonances, and additional theoretical calculations, mainly near the spin–orbit split thresholds, are highly desirable.

A further interesting field where calculations are worthwhile concerns the photoionisation from excited states of alkaline earths since a wealth of experimental data now exist (Aymar 1984). Although most recent experiments dealt with Ba, some results are available for Sr (Xu *et al* 1986, 1987, Zhu *et al* 1987). The data on the 5sns $^1S_0$–5pn's

$J = 1°$ and $5snd\ ^1D_2$–$5pn'd$ $J = 3°$ ($n > 10$) photoionisation spectra are of particular interest since these provide information not only on the positions and widths of resonances but also on branching ratios for autoionisation and on angular distributions of photoelectrons. These latter measurements provide a more sensitive test of the wavefunctions. Interpretation of the $5sns\ ^1S_0$–$5pn's$ $J = 1°$ spectra is in progress.

Acknowledgment

I wish to thank S Watanabe for his valuable discussions and critical reading of the manuscript. I am also grateful to J P Connerade and M L Ginter for providing figures and comments.

Note added. After submission of the manuscript, I received the new results obtained in Ca by Kim and Greene (1987). I am gratefully indebted to C H Greene for sending me this manuscript prior to publication. This paper confirms for Ca the conclusion for Sr, i.e. the simple (*jj*–*LS*) frame transformation allows one to adequately describe various effects of the spin-orbit interaction which stand out in the photoionisation spectra of Ca.

References

Altun Z, Carter S L and Kelly H P 1983 *Phys. Rev.* A **27** 1943
Aymar M 1984 *Phys. Rep.* 110 163
Aymar M, Luc-Koenig E and Watanabe S 1987 *J. Phys. B: At. Mol. Phys.* **20** 4325
Bartschat K, Rudge M R H and Scott P 1986 *J. Phys. B: At. Mol. Phys.* **19** 2469
Berry R S and Krause J L 1987 *Adv Chem. Phys.* in press
Brown C M and Ginter M L 1978 *J. Opt Soc. Am.* **68** 817
—— 1980 *J. Opt. Soc. Am.* **70** 87
Brown C M, Longmire M S and Ginter M L 1983 *J. Opt. Soc. Am.* **73** 985
Connerade J P, Baig M A, Garton W R S and Newsom G H 1980 *Proc. R. Soc.* A **371** 295
Cowan R D 1981 *The Theory of Atomic Structure and Spectra, Los Alamos series in basic and applied sciences* (Stanford, CA: University of California Press)
Esherick P 1977 *Phys. Rev.* A **15** 1920
—— 1983 *Rep. Prog. Phys.* **46** 97
Fano U 1975 *J. Opt. Soc. Am.* **65** 979
Fano U and Rau A R P 1986 *Atomic Collisions and Spectra* (Orlando, Fl: Academic)
Garton W R S and Codling K 1968 *J. Phys. B: At. Mol Phys.* **1** 106
Garton W R S, Grasdalen G L, Parkinson W H and Reeves E M 1968 *J. Phys. B: At. Mol. Phys.* **1** 114
Greene C H 1983 *Phys. Rev.* A **28** 2209
—— 1985 *Phys. Rev.* A **32** 1880
Greene C H, Fano U and Strinati G 1979 *Phys. Rev.* A **19** 1485
Greene C H and Jungen C 1985 *Adv. Mol. Phys.* **21** 51
Greene C H and Kim L 1987 *Phys. Rev.* A in press
Griffin D C, Andrew K L and Cowan R D 1969 *Phys. Rev.* **177** 62
Hudson R D, Carter V L and Young P A 1969 *Phys. Rev.* **180** 77
Kim L and Greene C H 1987 *Phys. Rev.* A to be published
Krause J L and Berry R S 1985 *J. Chem. Phys.* **83** 5153
Lee C M and Lu K T 1973 *Phys. Rev.* A **8** 1241
Lu K T 1971 *Phys. Rev.* A **4** 579
Lutjens 1973 *Z. Naturf.* **28a** 260
Moore C E 1952 *Atomic Energy Levels* NBS Circular No 467 Vol II (Washington, DC: US Govt Printing Office)
O'Mahony P F 1985 *Phys. Rev.* A **32** 908
O'Mahony P F and Greene C H 1985 *Phys. Rev.* A **31** 250
O'Mahony P F and Watanabe S 1985 *J. Phys. B: At. Mol. Phys.* **18** L239

Parkinson W H, Reeves E M and Tomkins F S 1976 *J. Phys. B: At. Mol. Phys.* **9** 157
Scott P, Kingston A E and Hibbert A 1983 *J. Phys. B: At. Mol. Phys.* **16** 3945
Seaton M J 1983 *Rep. Prog. Phys.* **46** 167
Ueda K 1987 *Phys. Rev.* A **35** 2484
Watanabe S 1986 *J. Phys. B: At. Mol. Phys.* **19** 1577
Xu E Y, Zhu Y, Mullins O P and Gallagher T F 1986 *Phys. Rev.* A **33** 2401
—— 1987 *Phys. Rev.* A **35** 1138
Zhu Y, Xu E Y and Gallagher T F 1987 *Phys. Rev.* A submitted